On the hot and cold autosolitons in dissipative semiconductor structures

2005 J. Phys.: Condens. Matter 17 3843

(http://iopscience.iop.org/0953-8984/17/25/011)

INSTITUTE OF PHYSICS PUBLISHING JOURNAL OF PHYSICS: CONDENSED MATTER

J. Phys.: Condens. Matter **17** (2005) 3843–3850 doi:10.1088/0953-8984/17/25/011

On the hot and cold autosolitons in dissipative semiconductor structures

I K Kamilov, A A Stepurenko[1] and A S Kovalev

Institute of Physics of Daghestan Science Center, Russian Academy Science, M Yaragskogo street, 94, Makhachkala, 367003, Russia

E-mail: ask@iwt.ru (A S Kovalev)

Received 7 February 2005, in final form 13 May 2005
Published 10 June 2005
Online at stacks.iop.org/JPhysCM/17/3843

Abstract

It is experimentally shown that in bulk InSb and Te single crystals, during the formation and excitation of the dissipative structure in the non-equilibrium electron–hole plasma, in the case of a presence of longitudinal autosolitons, the carrier concentration decreases outside the autosolitons, while it increases in the case of transverse autosolitons.

The longitudinal autosolitons, forming in the non-equilibrium electron–hole plasma by Joule heating, are considered to be cold, and the transverse autosolitons to be hot.

1. Introduction

The theoretical investigations of Kerner and Osipov [1–7] have shown that the localized regions of the extreme carrier concentration and temperature, i.e. thermodiffusion autosolitons, can be produced by applying an additional perturbation in the non-equilibrium excited electron–hole plasma (dissipative system). The parameters of these autosolitons are independent of the initial external perturbation energy, and are estimated by dissipative system parameters.

In a dense electron–hole plasma, $(\mu_e, \mu_p \sim T^{3/2})$, in the presence of an external electric field, the autosolitons appear as current sheets directed along the applied electric field (longitudinal autosolitons [3, 4]), while in an electron–hole plasma with a lower density the autosolitons are formed as strong electric field layers oriented normally to the lines of current (across autosolitons [3–5]).

In such a way, a dissipative structure is created, where any type of autosolitons can be present.

There are experimentally detected and investigated autosolitons in the electron–hole plasma induced by impact ionization or injection in n-GaAs [8, 9]. Moving autosolitons

[1] Author to whom any correspondence should be addressed.

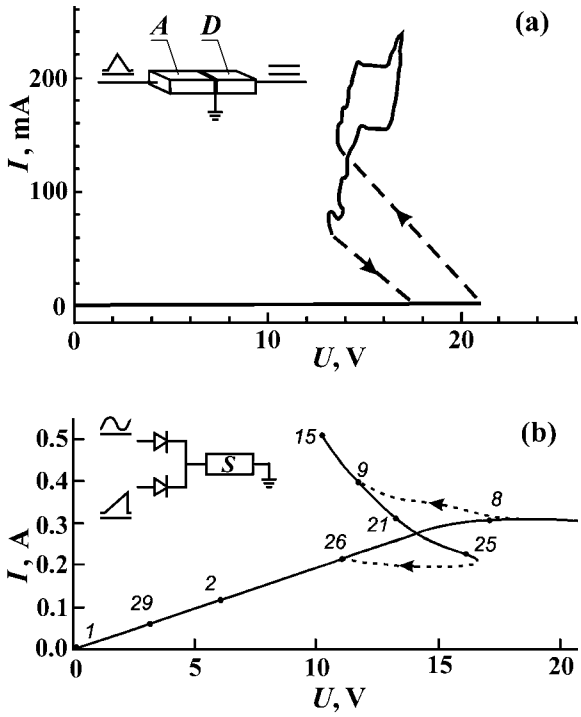

Figure 1. (a) Scheme of the InSb sample: activator (A) and detector (D), scheme of the sample connection in a circuit, and the current–voltage characteristic of the activator. (b) Scheme of the sample connection in a circuit, and quasi-steady current–voltage characteristic of the Te sample.

are found in the plasma obtained by photogeneration in n-Ge [10] and by Joule heating in InSb [11, 12].

A localized region of high temperature and low carrier concentration (hot autosoliton) and a localized region of low temperature and high carrier concentration (cold autosoliton) have been described in [13].

Being regions of high electric field, i.e. of low conductivity, the transverse autosolitons that are static or moving in the electric field are in fact hot autosolitons. The dynamics of generation and subsequent evolution of both static and moving transverse autosolitons were experimentally researched using potential probing [10, 12]. Experimental studies revealing the physics of longitudinal autosolitons have not been reported.

2. Experiment

The aim of this study was to gain insight into the character of the longitudinal autosoliton formed in electron–hole plasma by Joule heating. InSb samples of various sizes with a carrier concentration $p = 2$–4×10^{12} cm^{-3} and the mobility $\mu \sim 4000$ cm^2 V^{-1} s^{-1}, and Te samples with a carrier concentration $p = 1.45 \times 10^{14}$ cm^{-3} and the mobility $\mu \sim 2400$ cm^2 V^{-1} s^{-1} at $T = 77$ K were studied. Copper wires, soldered using indium, were used as the current lead. The InSb sample was divided into two regions (figure 1(a)): activator (A) and detector (D). Autosolitons were excited in the activator by applying a saw-toothed pulse voltage for 50 s, as was described in [11, 12]. The current–voltage characteristic of the activator testifying

occurrences of a steady current filament is shown in figure 1(a). A constant voltage of 6.8 V was supplied to the detector for the detection of the current I variation proceeding through the detector, i.e. the change of carrier concentration $n \sim I$ in the detector. Any variations of the carrier concentration in the activator have an effect on the detector conductivity.

Acoustic probing is another method for researching the dissipative structure. It is well known [14–19] that a pronounced acoustoelectric effect is observed in Te. In a high electric field when the carrier drift velocity v_d becomes higher than the phase velocity of sound v_s, phonons are generated which interact with the charge carrier in the crystal. It is experimentally shown [16] that acoustoelectronic interaction in tellurium depends linearly on the charge carrier concentration.

$$\gamma = Cn, \tag{1}$$

where

$$C = \frac{K^2 e^3 V_S^4 \beta}{2\varepsilon k^2 T^2 \omega^2 \mu},$$

K is the electromechanical coupling coefficient, $\beta = v_d/v_s - 1$ is the drift parameter, ε is the dielectric constant, ω is the cyclic frequency of the generated sonic waves, and μ is the charge carrier mobility.

$\omega > (\omega_c \omega_d)^{1/2}$, $\omega_c = en\mu/\varepsilon$ is the dielectric relaxation frequency, $\omega_d = ev_s^2/\mu kT$ is the diffusion frequency. The equation for C at $K^2 = 0.2$, $v_s = 2 \times 10^5$ cm s^{-1}, $\mu = 2.4 \times 10^3$ cm^2 V^{-1} s^{-1}, $n = 1.45 \times 10^{14}$ cm^{-3}, $E = 100$ V cm^{-1}, $\beta = 0.2$, $\varepsilon = 10$, $T = 77$ K, $\omega_c = 4.35 \times 10^9$ s^{-1}, $\omega_d = 3.5 \times 10^9$ s^{-1}, $\omega > 3.9 \times 10^9$ s^{-1} gives: $C = 2.85 \times 10^{-8}$ cm^3 s^{-1}.

Longitudinal autosolitons are excited and maintained by the quasi-constant voltage applied to the sample. The current–voltage characteristic is shown in figure 1(b). The dynamic current–voltage characteristic with a non-linear part caused by the acoustoelectric effect is obtained by application of a strong triangular pulse with a duration of the electric field $\tau = 20$ μs to the same sample. As every current–voltage characteristic point is fixed at quasi-constant current (figure 1(b)), the dynamic current–voltage characteristic can be measured at a constant current flow through the same sample.

3. Results and discussion

Experimental results for the InSb samples are shown in figures 1(a) and 2. The activator current–voltage characteristic in the saw-toothed voltage field before the formation and excitation of autosolitons is presented in figure 1(a). All parts of current–voltage characteristic, except those marked by arrows, are reproducible and stable in time. Oscillograms of the time dependence of the activator current I_A, corresponding to this current–voltage characteristic, and the change of the detector conductivity are shown in figures 2(a) and (b) respectively. The increase of the detector conductivity in the AB section (figure 2(b)) is the result of an increase of the carrier concentration activator due to Joule heating. But the conductivity of the activator did not change because of decrease of charge carrier mobility in it. The further increase of heating gives rise to intrinsic conductivity in the activator, and due to this fact an abrupt increase of the non-equilibrium carrier concentration occurs (figure 2(a), section BC). Due to diffusion of the non-equilibrium carriers, the detector conductivity also abruptly increases (figure 2(b), section BC).

The section BC indicates that electron–hole plasma is formed in the activator and is transformed into the dissipative structure when the voltage increases, i.e. electron–hole plasma

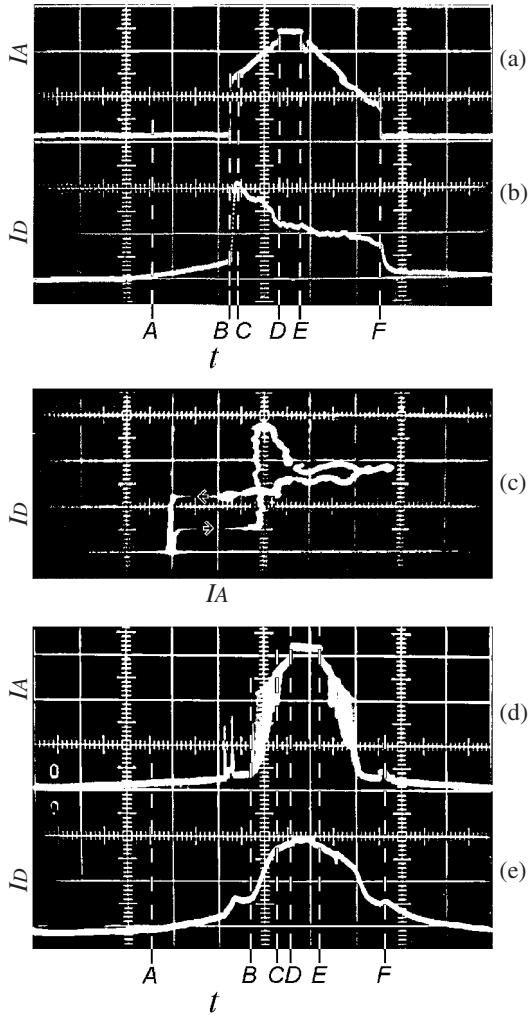

Figure 2. Oscillograms: (a) the time dependences of the activator current; (b) the time dependences of the detector conductivity under excitation of the longitudinal autosolitons in the activator. (Units: $I_A = 0.1$ A/div, $I_D = 2 \times 10^{-4}$ A/div, $t = 5$ s/div.) (c) The dependence of the detector conductivity on the activator current. (Units: $I_A = 5 \times 10^{-2}$ A/div, $I_D = 1.5 \times 10^{-4}$ A/div, $t = 5$ s/div.) Oscillograms: (d) the time dependences of the activator current; (e) the detector conductivity under the excitation of the transverse autosolitons in the activator. Units of the I_A and I_D current measurements are the same as in oscillograms (a) and (b).

stratifies into localized regions of the extreme temperature. The carrier concentration in these regions is presented as current sheets and electric field strata [1–7]. One can see in figure 2(a) (section CD) the current sheet (longitudinal autosoliton) forms. The external applied voltage controls the magnitude of the current. If the localized regions of decreased and increased carrier concentration are formed in the sample bulk then the carrier concentration should increase and decrease correspondingly in the remaining sample volume, resulting in an increase and decrease of the detector conductivity. In this case the experiment shows that the detector conductivity decreases in a step-like manner (figure 2(b), section CD), while the activator current increases (figure 2(a), section CD). This means that the carrier concentration decreases

in the activator volume as the dissipative structure is forming and exciting. It points to the saturation of localized regions by the charge carrier, the temperature of which drops relative to the remaining bulk sample [13]. We suppose that the step-like decrease of the detector conductivity indicates that additional longitudinal autosolitons are formed abruptly with the increase of applied voltage, i.e. increase of the dissipative structure excitation level. In this case, an abrupt decrease of the carrier concentration in the activator volume is observed.

The dependence of the detector conductivity σ_{D} upon the activator current I_{A} is presented in figure 2(c). One can see that the detector conductivity, and, therefore, the carrier concentration essentially decreases in the bulk activator, when the current of the longitudinal autosoliton in the activator increases. The jump of the detector conductivity does not coincide with the current jump in the activator because of the delay of the detector conductivity change in relation to the electron–hole plasma generation in the activator. As we see, when the current sheet increases in the activator, the carrier concentration decreases in the remaining part of the activator.

The oscillogram of the time dependence of the current in the activator and the detector conductivity at voltages, when electric field strata (transverse autosoliton) moving along the sample excite in the activator, and the current oscillations in the external circuit are presented in figure 2(d) (section BC). One can see that the decrease of detector conductivity does not occur if there are moving autosolitons in the activator. Moreover, the detector conductivity increases (figure 2(e) section BC); this involves an increase of charge carrier concentration in the bulk activator.

The experimental results for the Te samples are given in figures 1(b), 3 and 4. The well-reproducible quasi-constant current–voltage characteristic measured at the voltage change of the electric field in the direct and reverse directions is shown in figure 1(b). The dashed lines mark time-unstable parts.

Dynamic current–voltage characteristics were measured at a constant-current flow through the sample corresponding to the different parts of the quasi-constant current–voltage characteristic (points 1–29). Points 1–8, 26–29 are plotted on the ohmic part of the quasi-constant current–voltage characteristic (figure 1(b)), and points 9–25 are plotted on the part of the quasi-constant current–voltage characteristic at the applied voltages when the longitudinal autosoliton is formed (AS-sample). In figure 3(a) one can see the dynamic current–voltage characteristic measured at a current corresponding to points 1, 8, 15, 25 and 26 in the quasi-constant current–voltage characteristic (figure 1(b)). As one can see in figure 3(a) (1, 8) the current–voltage characteristics are identical, although they are measured at ohmic current flow of different values. The dynamic current–voltage characteristics, already in the presence of the autosoliton, are shown in the oscillograms 15, 21, 25 (figure 3(a)). The acoustoelectric oscillations disappear. The slope angle of the non-linear current–voltage characteristic increases, which indicates a decreasing of the interaction between the charge carrier and acoustoelectric oscillation. This occurs owing to the decrease of the phonon-flux density that is caused by a reduction of the charge carrier concentration in the sample bulk containing autosolitons. The carrier concentration may be determined from the experimental dynamic current–voltage characteristic. The current density at an electric field that is higher than the critical value $E > E_{\mathrm{th}}$ (figure 3(b)) under saturation conditions ($\beta = 0$) is equal to $j_{\mathrm{S}} = en_{\mathrm{a}}\mu E = en_{\mathrm{a}}v_{\mathrm{s}}$, where $n_{\mathrm{a}} = n$.

If $\alpha > \beta > 0$, only a fraction of the carriers n_{a} are involved in the acoustoelectronic interaction; the other fraction n_0 is involved in the ohmic current. As a result, we obtain

$$j_{\mathrm{a}} = en_{\mathrm{a}}\mu E + en_0\mu E = en_{\mathrm{a}}v_{\mathrm{s}} + en_0\mu E, \qquad (n = n_{\mathrm{a}} + n_0). \tag{2}$$

In this case, on the one hand we have $\frac{j-j_{\mathrm{a}}}{j-j_{\mathrm{S}}} = \frac{n_{\mathrm{a}}}{n}$, where $j = \sigma E = en\mu E$.

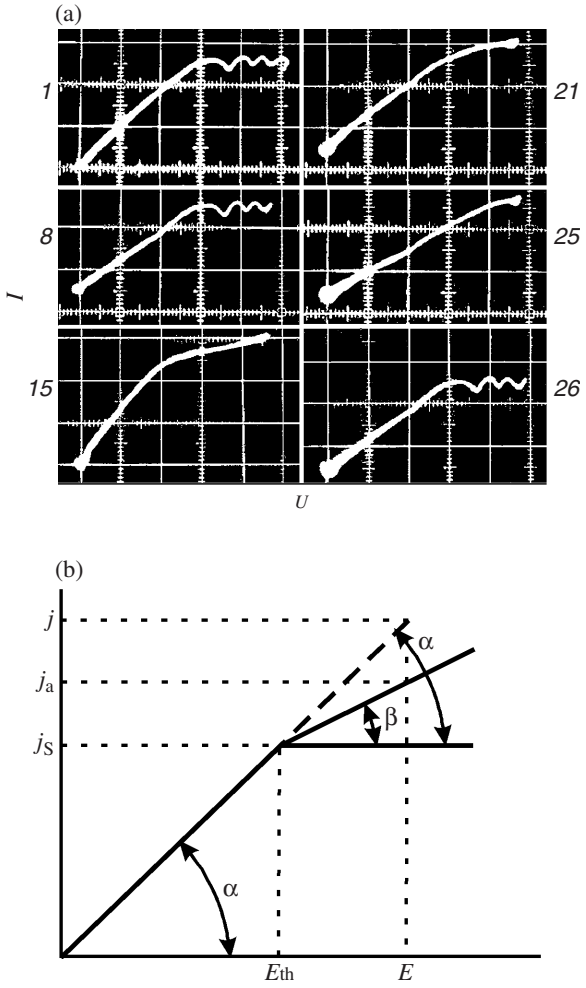

Figure 3. (a) Oscillograms of the dynamic current–voltage characteristics of the Te sample. Units: $I = 33 \times 10^{-2}$ A/div, $U = 25$ V/div. (b) Typical current–voltage characteristic of Te under conditions of acoustoelectronic interaction.

On the other hand, according to figure 3(b) we obtain $\frac{j-j_a}{j-j_S} = \frac{\tan\alpha - \tan\beta}{\tan\alpha}$.

Therefore $\frac{n_a}{n} = \frac{\tan\alpha - \tan\beta}{\tan\alpha}$. In the experimental dynamic current–voltage characteristic of the ohmic sample (figure 3(a) (1 and 8)) $\beta > 0$, so that $n_a/n = 1$. For the AS-sample (figure 3(a) (15, 21, 25))

$$\frac{n_{aAS}}{n} = \frac{\tan\alpha_{AS} - \tan\beta_{AS}}{\tan\alpha_{AS}}, \tag{3}$$

where α_{AS} and β_{AS} are the slope angles of the linear and non-linear parts of the dynamic current–voltage characteristic of the AS-sample (figure 3(a) (15, 21, 25)). Angles α_{AS} and β_{AS} depend on the excitation level of the autosoliton, i.e. on the current I_A. The dependence of the change of the carrier concentration n_a/n, involved in the acoustoelectric interaction, upon the current autosoliton is drawn in figure 4. A steady decrease of n_a/n is observed with a reduction of the current autosoliton.

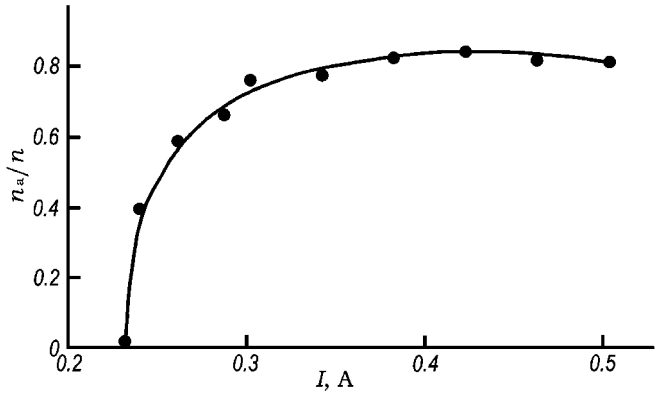

Figure 4. The dependence of carrier concentration ratio n_a/n (carriers are involved in the acoustoelectronic interaction) on the autosoliton current in the Te samples.

4. Conclusion

It was experimentally shown that the carrier concentration changed in a bulk sample of InSb and Te single crystals during the formation and excitation of dissipative structure by a strong electric field in the electron–hole plasma created by Joule heating. In the case when there were only longitudinal autosolitons in the dissipative structure, the carrier concentration decreased with increase of excitation level of these autosolitons. This is conditioned by the increase of the carrier concentration in the localized regions and by the decrease of their temperature (cold autosolitons) [13].

When there were transverse autosolitons in the dissipative structure (InSb samples) the carrier concentration in the bulk sample became higher, and it increased with increasing the excitation level of these autosolitons. Since the transverse autosolitons were localized regions with reduced charge carrier concentration and high temperature (hot autosoliton), the remaining part of the bulk sample was more saturated by the charge carriers.

It could be considered that longitudinal autosolitons, forming in the non-equilibrium electron–hole plasma created by the Joule heating, were cold.

Experimental studies of the limiting tolerance current of the longitudinal autosoliton in InSb showed the stability of this autosoliton at a current density up to 6×10^6 A cm^{-2}. The large current density of longitudinal autosolitons was conditioned, first of all, by a decrease of the electron temperature in the autosoliton centre relative to the outlying regions due to the increase of the carrier concentration in the localized region—autosoliton. This follows from the equation of thermal balance between the electrons in autosoliton and the lattice [1]:

$$W = \sigma E^2 = n(T_e - T_o)/\tau_\varepsilon, \tag{4}$$

where $W = \sigma E^2$ is the specific power supplied to the specimen, T_e is the electron effective temperature, T_o is the lattice effective temperature, and τ_ε is the relaxation time of the electrons energy.

References

[1] Kerner B S and Osipov V V 1976 *Zh. Eksp. Teor. Fiz.* **71** 1542
[2] Kerner B S and Osipov V V 1985 *Zh. Eksp. Teor. Fis. Pis.* **41** 386
[3] Kerner B S and Osipov V V 1973 *Zh. Eksp. Teor. Fiz. Pis.* **18** 122

[4] Kerner B S and Osipov V V 1979 *Fiz. Tekh. Poluprov.* **13** 891
[5] Kerner B S and Osipov V V 1979 *Fiz. Tverd. Tela* **21** 2342
[6] Kerner B S and Osipov V V 1979 *Fiz. Tekh. Poluprov.* **13** 721–34
[7] Dubitskii A L, Kerner B S and Osipov V V 1986 *Fiz. Tverd. Tela* **28** 1290–5
[8] Kerner B S and Sinkevich V F 1982 *Zh. Eksp. Teor. Fiz. Pis.* **36** 359
[9] Kerner B S, Osipov V V, Romanenko M T and Sinkevich V F 1986 *Zh. Eksp. Teor. Fiz. Pis.* **44** 77
[10] Vinoslavsky M N 1989 *Fiz. Tverd. Tela* **31** 315–8
[11] Stepurenko A A 1994 *Fiz. Tekh. Poluprov.* **28** 402
[12] Kamilov I K and Stepurenko A A 1996 *Phys. Status Solidi* b **194** 643
[13] Gafijchuk V V, Kerner B S, Osipov V V and Yuzhanin A G 1988 *Fiz. Tekh. Poluprov.* **22** 2051
[14] Ishiguro T and Tanaka T 1967 *Japan. J. Appl. Phys.* **6** 864
[15] Quentin G 1967 Phenomenes acoutoelectriques dans les semiconducteurs piezoelectriques—Application at tellure *These de doctorat d'etetes sciences physiques,* Paris, p 126
[16] Shiosaki T, Matsumoto H, Chiharo H and Kawabata A 1973 *Japan. J. Appl. Phys.* **12** 337
[17] Kuzmany H 1974 *Phys. Status Solidi* a **25** 9
[18] Kuzmany H and Liederer W 1973 *Phys. Status Solidi* a **15** 121
[19] Stepurenko A A 1982 *Author's Abstract of Candidate's Dissertation* Makhachkala